A comparison study of dislocation density, recrystallization and grain growth among nickel, FeNiCo ternary alloy and FeNiCoCrMn high entropy alloy

P. Thirathipviwat[a*], G. Song[b], J. Jayaraj[c], J. Bednarcik[d], H. Wendrock[a], T. Gemming[a], J. Freudenberger[a,e], K. Nielsch[a,f,g], J. Han[a]

[a] *Leibniz Institute of Solid State and Materials Research (IFW Dresden), Helmholtzstr. 20, 01069 Dresden, Germany*

[b] *Division of Advanced Materials Engineering, Kongju National University, Cheonan, 330-717 Chungnam, Republic of Korea*

[c] *Material Science, Dalarna University, Högskolegatan 2, 791 31 Falun, Sweden*

[d] *DESY, Notkestraße 8, D-22607 Hamburg, Germany*

[e] *Institute of Materials Science, Technische Universität Bergakademie Freiberg, Gustav-Zeuner-Str. 5, D-09599 Freiberg, Germany*

[f] *Institute of Materials Science, Technische Universität Dresden, 01062 Dresden, Germany*

[g] *Institute of Applied Physics, Technische Universität Dresden, 01062 Dresden, Germany*

**Corresponding author. E-mail address: p.thiratipviwat@ifw-dresden.de, pthirathipviwat@gmail.com*

Abstract

The microstructural evolutions in terms of dislocation density, annealing twin density as well as with respect to microstructural changes due to recrystallization and grain growth were investigated in pure Ni, equiatomic FeNiCo alloy, and FeNiCoCrMn high entropy alloy (HEA) during the thermomechanical process. All samples were single phase and showed a face-centered cubic (FCC) lattice structure. This was maintained during thermomechanical processing comprising of cold swaging by 85 % reduction of cross-sectional area and subsequent annealing at 800°C. The level of dislocation accumulation during cold swaging increased with the number of constituent elements. The FeNiCoCrMn HEA obtained the highest dislocation density, followed by the FeNiCo and Ni, respectively. After the annealing at 800°C for 0.5 hours, all samples achieved the large fraction of recrystallized grains with minor fraction of substructured grains and no deformed grain. The FeNiCoCrMn HEA obtained the smallest recrystallized grain size (~ 5 μm) after the annealing at 800°C for 0.5 hours. This could be a result of the highest dislocation density generated during cold swaging prior to the annealing. The prolonged annealing at 800 °C for up to 24 hours

led to a grain growth for all the samples, however, at different growth rates. The FeNiCoCrMn HEA revealed the lowest rate of grain growth, but the microstructural changes during the annealing were not significantly different between the FeNiCo and Ni samples. Besides the effect of the number of constituent elements, the type and the combination of constituent elements have an effect on the microstructural evolution during the annealing.

Keywords: High entropy alloys, Dislocation density, Grain growth, EBSD, X-ray diffraction

1. Introduction

The equiatomic FeNiCoCrMn high entropy alloy (HEA), also termed as Cantor's alloy, was firstly introduced in 2004 [1], consisting of a single face-centered-cubic (FCC*)* structured solid solution phase. The HEAs are designed based on the concept of entropic stabilization associated with a large number of constituents in order to stabilize a disordered solid solution over completing intermetallic compounds [2-5]. As a result, HEAs are claimed to present exceptional microstructural stability [3, 6]. However, recent studies indicate that most HEAs are not stable as single solid solution within entire temperatures range of the solid state [4]. It is reported that the FeNiCoCrMn HEA can be stabilized as a single phase HEA up to 72 h at 1000 °C [6]. The good thermal phase stability and an excellent malleability [7] of the FeNiCoCrMn HEA facilitate to tune mechanical properties and other properties by microstructural control with a conventional processes [8]. It is well known that the properties of materials, especially mechanical properties, are closely correlated to the microstructure and processing conditions [4, 8]. Many works state superior properties of HEAs [9]; they are expected to show different microstructural features from conventional metallic materials [10, 11].

The remarkable workability and high fracture toughness of the FeNiCoCrMn HEA [12, 13] are attributed to large work hardenability [2, 14]. The large work hardenability is assumed to be caused by dislocation pile-ups, dislocation motion and nanotwinning [2, 14]. The characterization of dislocation motion in HEAs have been addressed in the literatures [15-17]. Many studies indicate that the deformation mechanism of HEAs is similar to FCC concentrated binary solid solution alloys and metals [18, 19]. In plastic deformation for common FCC alloys, the dislocations densely glide on close-packed {111} planes [19]. However, the quantitative analysis of dislocation is still needed to understand deformation behavior in HEAs [15]. In this study, the rotary swaging was applied to deform the samples in order to study an accumulation of dislocation. Moreover the rotary swaging associated with large hydrostatic stresses delays brittle fracture and allows the accumulation of high plastic strain [20].

It is well know that the microstructure depends on the condition of manufacturing route. The level of dislocation density during the plastic deformation prior to the annealing determines a driving force for recrystallization [21]. Moreover, the slow diffusion kinetic is assumed to have an effect on microstructure features of HEAs such as excellent thermal phase stability, homogeneous microstructure and high resistance to grain coarsening [10, 20, 22]. It is reported that the full recrystallization in the FeNiCoCrMn HEA occurs first at 800°C of annealing after 84 - 96% reduction of thickness under plastic deformation [23]. Hence, in this study, the microstructural changes in terms of a recrystallization and grain growth as well as annealing twin density were studied through the isothermal annealing at 800°C after 85% reduction of cross-sectional by cold rotary swaging. The less chemical complex FCC solid solution samples, such as the FeNiCo alloy and pure Ni, were investigated in a comparison with FeNiCoCrMn HEA.

2. Experimental procedure

The equiatomic FeNiCoCrMn HEA, the equiatomic FeNiCo sub-alloy and pure Ni sample were prepared from pure elements with purities higher than 99.9 wt% by arc-melting under a Ti-gettered high-purity argon atmosphere. The pre-alloyed ingots were flipped over and remelted at least 3 times to ensure chemical homogeneity. The pre-alloyed ingots were subsequently transferred to an in-house built cold-crucible device to be remelted and cast into water-cooled 6 mm diameter cylindrical Cu molds.

The samples were encapsulated in evacuated and Ar backfilled (~ 200 mbar) quartz tubes prior to homogenization and annealing. The cast rods were homogenized at 1000 °C for 12 h, followed by water quenching. Cold rotary swaging was performed on homogenized samples with a cross-sectional reduction of 19% per step until a total reduction of 85% was reached. For this purpose, a four headed rotary swager was utilized. After swaging, the rods were encapsulated in quartz tubes (as described before) and then subsequently isothermal annealed at 800 °C for different times (0.5 to 24 hours), followed by water quenching.

High energy synchrotron X-ray diffraction was conducted in transmission geometry with E = 60 keV ($\lambda = 0.2067150$ Å) and $Q_{max} = 12$ Å^{-1} ($Q = 4\pi\sin\theta/\lambda$) of experimental setting at High Resolution Powder Diffraction Beamline P02.1 of DESY in Hamburg, Germany. The X-ray diffraction patterns were analyzed by Williamson-Hall method to estimate the dislocation density. To allow for microstructural characterization of the samples, longitudinal sections were cut and subsequently ground with SiC papers with reducing grit sized up to P4000 and further polished with diamond suspensions with a particle size down to 0.25 μm. A final polishing step was performed using with colloidal silica (particle size 0.05 μm) on a vibratory polisher. The microstructure was examined by a scanning electron microscope (SEM: Zeiss

Gemini 1530) equipped with an energy-dispersive X-ray spectrometer (EDX: Bruker XFlash 4010) and an electron backscatter diffraction detector (EBSD: Bruker e-Flash HR). Grain size, twin boundary density, and recrystallized fraction derived from misorientation distribution were determined via EBSD post-processing CHANNEL 5 software (Oxford instruments). An EBSD map was acquired with a step size of 0.5 – 1.0 μm. A grain was defined as an aggregate of neighboring data points having relative misorientations smaller than 2°. For grain size determination, Σ3 twin boundaries were ignored and a critical misorientation (θ) of 10° was used to determine the grain and sub-grain according to the manual of CHANNEL 5 software. Typically, grain boundaries with misorientations between 2˚ and 10˚ are considered as subgrains and grain boundaries with misorientations larger than 10° are classified as high-angle grain boundaries [24]. The concentration of twin boundaries was determined by the calculation of $\Sigma 3^n$, n = 1, 2, 3 in coincidence site lattice notation [25, 26]. The deformed, substructured and undeformed (recrystallized) fractions was evaluated by misorientation distribution. If the internal average misorientation angle within the grain exceeded the minimum angle (2°) to define a subgrain, the grain was classified as being "deformed". If grains consist of subgrains whose internal misorientation was under 2° but the misorientation from subgrain to subgrain was above 2°, these grains were classified as "substructured". The rest of grains was classified as "undeformed grains".

3. Results and discussion

3.1 Dislocation density storage during cold swaging

Figure 1 presents the high energy synchrotron X-ray diffraction patterns of FeNiCoCrMn, FeNiCo and Ni samples after 85% cross-section area reduction of cold-swaging. The X-ray patterns of these samples are identified as a single face-centered cubic (FCC) structure phase without secondary phases, which indicates that FeNiCoCrMn and FeNiCo samples retain single phase after cold swaging. The peak positions are shifted with alloying, indicating an increase of the lattice parameter from Ni and FeNiCo to FeNiCoCrMn. The Rietveld analysis was done for the Cu structure type with the help of the FULLPROF code [27, 28]. The atoms were placed on the Wyckoff positions 4a (0,0,0) with an occupancy according to the stoichiometry. The Rietveld analysis involved the lattice parameter, the overall isotropic temperature factor, as well as two profile parameters describing the contribution of the small crystallite size and the variation of the interplanar spacing to the XRD line broadening. The Rietveld analysis yielded a lattice parameter of the samples to be 3.5207, 3.5690 and 3.5942 Å for Ni, FeNiCo and FeNiCoCrMn, respectively.

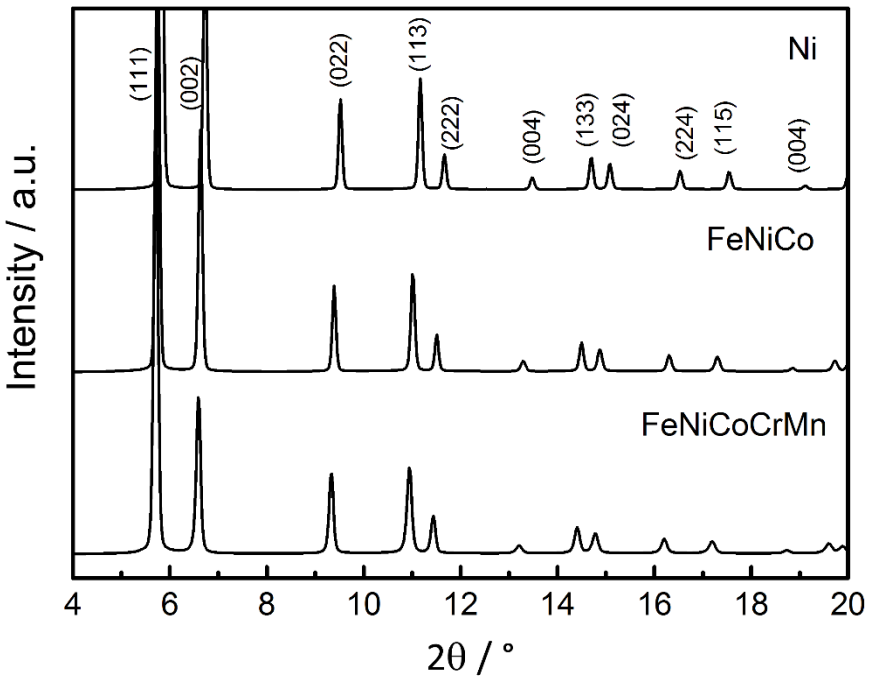

Figure 1. Synchrotron X-ray diffraction patterns of the as-swaged FeNiCoCrMn, FeNiCo and pure Ni samples.

The synchrotron X-ray diffraction patterns of the cold-swaged samples in Fig. 1 were analyzed using Williamson-Hall [29, 30] and Williamson-Smallman methods [31] to determine dislocation density stored during the swaging process. Specifically, Williamson and Hall suggested that the crystallite size (D_v) and lattice strain (ε_{str}) leads to a broadening of the diffraction peaks, as defined by the following equation,

$$\Delta\beta = \beta_D - \beta_{inst} = \beta_{size} + \beta_{strain} \quad (1)$$

$$\Delta\beta\cos\theta = \lambda/D_v + 4\varepsilon_{str}(\sin\theta) \quad (2)$$

where β_D is an integral breadth of Bragg peak (in radians 2θ), and β_{inst}, β_{size} and β_{strain} are the integral breadths dependent on instrumental, crystallite size and strain effects, respectively. The breadth of the Bragg peak is affected by a combination of both instrument and sample dependent effects, as shown in the equation (1). In this study, the instrumental broadening can be estimated by a calibration measurement with a LaB_6 standard sample. From the equation (2), the Williamson-Hall relationship between $(\beta_D - \beta_{inst})\cos\theta$ and $4\sin\theta$ can be plotted, as presented in Fig. 2 (a). The symbols in Fig. 2(a) represent the integral breadths and 2θ positions of the (111), (002), (022), (113), (222), (004), (133), (024), (224), (115) and (044) reflections. The grain (crystallite) size (D_v) and the micro lattice strain (ε_{str}) were derived from the y-intercept and the

slope of the linear fitting, respectively. After 85% reduction of cross-sectional area, the grain sizes were calculated as 98, 125, 156 nm for Ni, FeNiCo and FeNiCoCrMn sample, respectively, as listed in Table 1. The grain sizes were very small due to large degree of deformation. The values of the lattice strain (ε_{str}) were 0.1044, 0.1630 and 0.2196 % for Ni, FeNiCo and FeNiCoCrMn specimens, respectively. Moreover, these values of the lattice strain were adopted to evaluate the dislocation density (ρ) using the following equation proposed by Williamson and Smallman [31];

$$\rho = 16.1\frac{\varepsilon^2}{b^2} \quad (3)$$

where b is the magnitude of the Burgers vector. In the FeNiCoCrMn HEA, it is reported that plastic deformation occurs by planar dislocation glide on the normal *fcc* slip system, {111}<110> [19]. Therefore, the magnitude of the Burgers vector was calculated using the <110> slip direction [32] and is also listed in Table 1. Based on the calculated lattice strain and Burgers vector, the dislocation densities of the as-swaged samples (ρ) were calculated and summarized in Table 1. The dislocation densities of the Ni, FeNiCo and FeNiCoCrMn samples are 2.8 x 10^{14}, 6.7 x 10^{14} and 12.0 x 10^{14} m^{-2}, respectively. In general, dislocation density of annealed metals and alloys is about 10^{10} - 10^{12} m^{-2}, and can increase up to 10^{15} - 10^{16} m^{-2}, depending on the level of applied plastic strain [31, 33]. The stored dislocation densities of the samples after cold swaging are in the range of 10^{14} - 10^{15} m^{-2}, which supports the reliability of the current calculation.

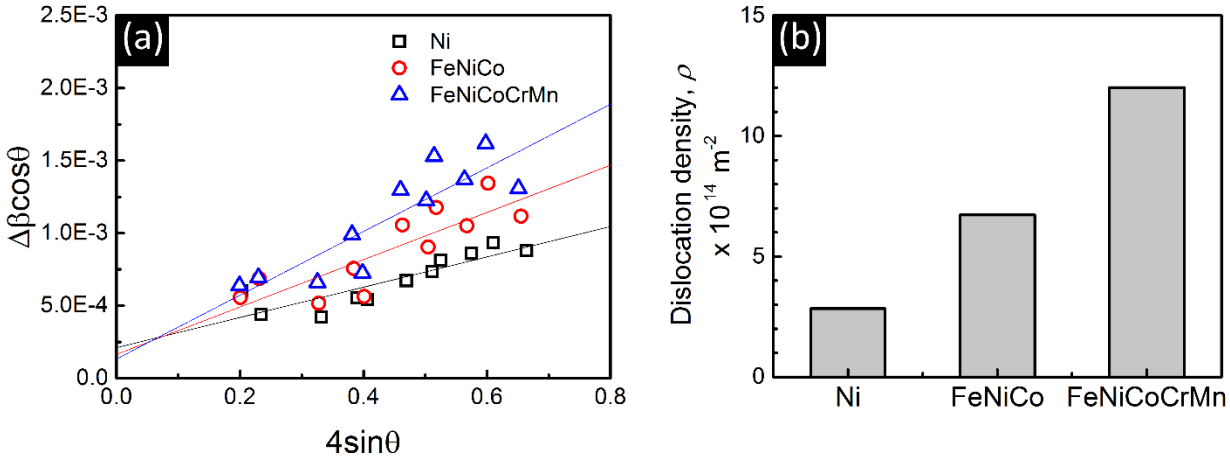

Figure 2. (a) Williamson-Hall analysis and (b) dislocation density of the as-swaged FeNiCoCrMn HEA, FeCoNi and pure Ni samples.

Table 1 lattice parameters (a), Burgers vector (b), grain (crystallite) size (D_v), lattice strain (ε), dislocation density (ρ) and stacking fault energy (γ) of as-swaged samples and homologous temperature for annealing at 800°C (1073K)

Alloys	a (Å)	b (Å)	D_v (nm)	ε (%)	ρ (x 10^{14} m^{-2})	γ (mJ/m^2)	T/T_m (T =1073K)
Ni	3.521	2.490	98	0.104	2.831	120 - 130 [34]	0.62
FeNiCo	3.569	2.524	125	0.163	6.719	31 [2]	0.63
FeNiCoCrMn	3.594	2.541	156	0.220	12.018	18 - 27 [35]	0.69

The calculated dislocation density of the FeNiCoCrMn HEA is higher than that of the FeNiCo alloy and also higher than the value observed for pure Ni. It is observed from the result that the number of constituent elements increase the dislocation density due to more chemical complexity from the Ni to FeNiCoCrMn HEA. Besides the number of constituent elements, the lattice distortion created by the random distribution of multiple principle elements in HEAs is often assumed to be an obstacle for dislocation motion and to affect the dislocation storage in HEAs. However, recent experimental investigations revealed that the level of the lattice distortion in the FeNiCoCrMn HEA was comparable to those of alloys containing smaller principle elements, such as FeNiCo alloy and Ni sample [36, 37]. Therefore, the role of the lattice distortion in the FeNiCoCrMn HEA on the interaction with dislocation activities is not expected to be dominant. Instead, there have been experimental and theoretical studies which relates the stacking fault energy (SFE) with the dislocation density, cell size and flow stress [38-40]. Based on these studies, a reduction of the SFE increases the total dislocation density and the flow stress, and promotes the splitting of a dislocation, which leads to the suppression of recombining the dissociated dislocations and annihilating the dislocations by cross-slip [32, 38]. The SFE of materials can be controlled by adjusting alloying elements [41]. Several studies have been reported regarding the effect of alloying elements to Ni-based alloys on the magnitude of the SFE. For example, the addition of Fe and Cr generally decreases the SFE, while the addition of Cr up to 25 wt. % reduces the SFE to 40 and 45 mJ/m^2 [42]. Meanwhile, the addition of Fe between 2.5 and 12.5 wt. % results in an average SFE value of 86 mJ/m^2 [11, 43]. Based on the previous experimental and theoretical investigations, the SFE of the alloys in the present study are obtained [2, 34, 35] and the values are indicated in Table 1. The FeNiCoCrMn HEA has a lower SFE (18 - 27 mJ/m^2) than the pure Ni and ternary FeNiCo alloy. Therefore, it is considered that the higher dislocation density of the FeNiCoCrMn HEA is strongly influenced by the SFE effect and also the large number of constituent elements.

3.2 Recrystallization and grain growth behaviors

Figure 3 presents SEM images of the pure Ni, FeNiCo, and FeNiCoCrMn samples recrystallized at 800°C for 0.5 hours after the 85% reduction of cross-sectional area. As observed in the SEM images, the as-annealed Ni and FeNiCo samples contain no secondary phase, whereas there was a small fraction of fine Cr-rich particles distributed in the recrystallized FeNiCoCrMn HEA [pointed by white arrows in Fig. 3 (c)]. Stepanov et al. reported that the volume fraction of the Cr-rich particles was about 0.3 % at 800°C annealing of the FeNiCoCrMn HEA [44]. Similarly, the fraction of the Cr-rich particle in this study is expected to be minor in the FeNiCoCrMn HEA. It was observed that all samples obtained recrystallized and equiaxed grains after the annealing at 800°C for 0.5 hours, and unrecrystallized grain was not seen. For further microstructural investigation, EBSD was used to analyze the fraction of deformed, substructured and undeformed (recrystallized) grains, as listed in Table 2. The result of the quantitative analysis supported the microstructure observation that the deformed grain was not remained in all sample after the annealing at 800°C for 0.5 hours. All samples achieved the large fraction of recrystallized grains after the annealing. The fractions of substructured grains in the as-annealed Ni and FeNiCo samples were measured as below 10%, while that of the FeNiCoCrMn HEA was detected as 20%. The presence of fine secondary phase particles in the HEA might inhibit recrystallization, then recovery occurs and induces the formation of substructured grains [45]. This might lead to a larger fraction of substructured grains in the HEA than in the Ni and FeNiCo samples. However, the microstructural analysis demonstrated that the fraction of substructured grains decreased to 5% for the HEA after the annealing for 2 h.

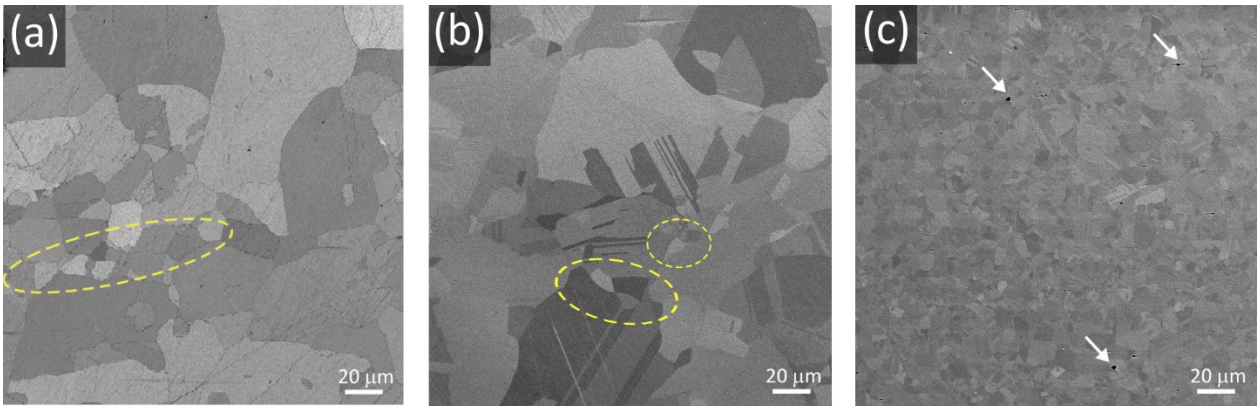

Figure 3. SE-SEM micrographs of (a) Ni, (b) FeNiCo and (c) FeNiCoCrMn alloys, annealed at 800°C for 0.5 hours. The yellow circles indicate the smaller grains surrounded by larger grains and the white arrows point Cr-rich particles.

Table 2 Microstructural analysis of the studied samples after the annealing at 800°C for 0.5 hours, evaluated on EBSD maps.

Alloys	Grain Size (μm)	Residual strain analysis			Twin Σ3 (%)
		Undeformed (%)	Substructured (%)	Deformed (%)	
Ni	26 ± 2	92	8	0	6
FeNiCo	21 ± 2	91	9	0	16
FeNiCoCrMn	5 ± 0	80	20	0	21

The average size of the grains after the recrystallization at 800°C for 0.5 h were estimated to be ~ 26 μm, ~ 21 μm, ~ 5 μm for the Ni, FeNiCo, and FeNiCoCrMn samples, respectively. Figure 4 presents grain size distribution of the annealed Ni, FeNiCo and FeNiCoCrMn samples subjected to annealing at 800°C for 0.5 h. For the FeNiCoCrMn HEA, the all grain sizes are measured as below 30 μm and the largest fraction of grain sizes are observed in the gran sizes between 0 – 5 μm. The grain sizes for the FeNiCo and Ni samples are more widely distributed than the HEA. On the grain size distribution maps of the FeNiCo and Ni samples, the bimodal distributions with two peaks are observed; the first peak is observed at the small grain size (10 - 20 μm) and another peak is seen at the grain sizes of 50 – 60 μm. The bimodal distributions imply the possible occurrence of abnormal grain growth in pure Ni and FeNiCo samples. This trend can be also observed in the microstructures of Figures 3 (a) and (b), where the growths of some grains in pure Ni and FeNiCo samples are possibly happened by consuming their adjacent and smaller neighbor grains [indicated by yellow circles in Figs. 3 (a) and (b)]. It was reported that abnormal grain growth in high-purity Ni and FeNiCo samples occurred at annealing temperatures lower than 0.68 T_m [11, 46], which is consistent with the current observation. This abnormal grain growth is attributed to grain boundary structural transformation [11], which leads to a partial change in the mobility of grain boundaries and allows them to migrate at a faster rate than other grain boundaries (which are not transformed). In this study, the Ni and FeNiCo samples were annealed at $0.62T_m$ and $0.63T_m$, respectively, and these annealing temperatures were lower than the temperature mentioned above (0.68 T_m). In contrast, the FeNiCoCrMn HEA exhibits the normal grain growth in the given annealing condition. The normal grain growth could be due to the higher annealing temperature ($0.69T_m$) for the FeNiCoCrMn HEA.

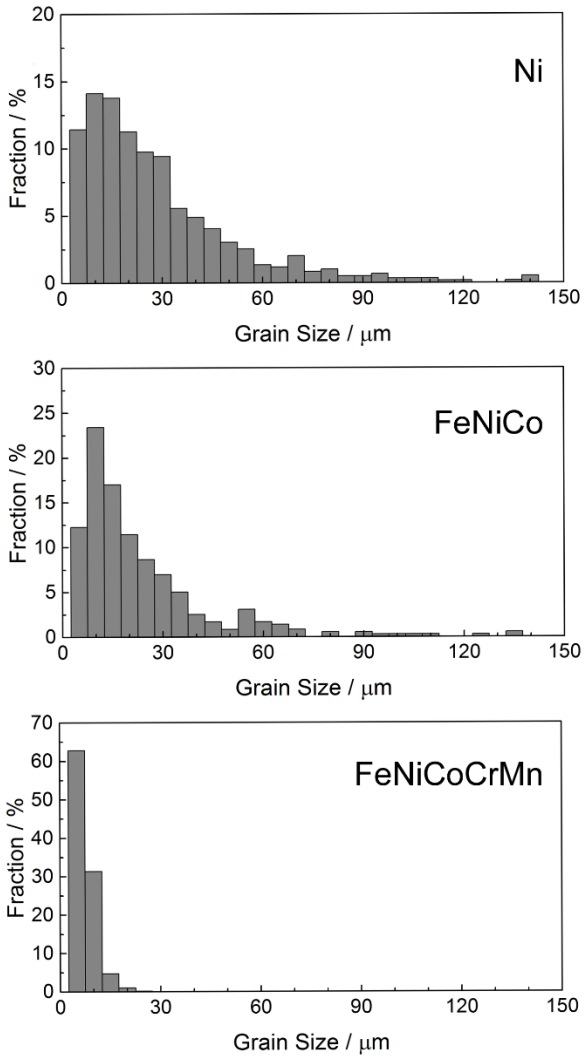

Figure 4. Grain size distribution of Ni, FeNiCo and FeNiCoCrMn samples after the annealing at 800°C for 0.5 hours.

The Ni, FeNiCo and FeNiCoCrMn samples subjected to annealing at 800 °C for 0.5 hours contain a high density of annealing twins, as observed in Fig. 3. Figure 5 exhibits EBSD grain boundary maps of Ni, FeNiCo and FeNiCoCrMn samples annealed for 0.5 hour. There are three kinds of twin boundaries, such as Σ3, Σ9, Σ27 in coincidence site lattice notation [25, 26], indicated by red, green and purple colors, respectively, in Fig. 5. The large amount of the Σ3 boundaries were observed after full recrystallization; while the quantities of Σ9 and Σ27 boundaries were relatively limited. Therefore, our focus was placed on the evolution of Σ3 boundaries for the twin formation. After 0.5 hour of annealing, the FeNiCoCrMn HEA obtained the highest amount (21%) of twin Σ3 boundaries followed by those of FeNiCo (16%) and Ni (6%) samples. The fraction of Σ3 boundaries is inversely proportional to the SFE of the samples. For example,

the FeNiCoCrMn HEA with the lowest SFE contains the highest fraction of the annealing twin boundaries. Therefore, it is considered that the lowering the SFE is effective to reduce the twin boundary energy [47-49], which stimulates the formation of annealing twinning boundaries.

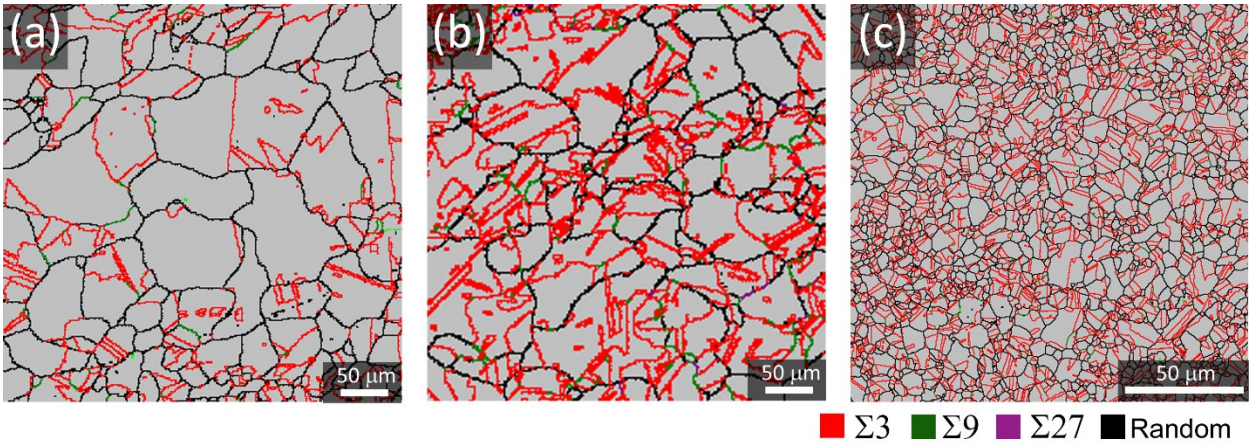

Figure 5. EBSD grain boundary maps of (a) Ni, (b) FeNiCo and (c) FeNiCoCrMn alloys, annealed at 800°C for 0.5 hours.

Figure 6 (a) displays the electron backscattered diffraction (EBSD) images of the Ni, FeNiCo and FeNiCoCrMn samples subjected to annealing at 800 °C for 0.5, 2 and 24 hours following the swaging process. As the annealing time increases, the sizes of recrystallized grains generally increase, as presented in Figure 6 (b). In the Ni and FeNiCo samples, the recrystallized grain sizes are gradually changed between 0.5 and 2 hours of the isothermal annealing. It should be mentioned that abnormal grain growth is observed in the Ni and FeNiCo samples; thus, average grain size could be deviated dependent on the measured area. However, it is consistent with the microstructural observation that the grain sizes of the Ni and FeNiCo are similar between 0.5 and 2 hours of the annealing, as exhibited in Fig. 6 (a). After 24 hours of annealing, the grain sizes of the Ni and FeNiCo samples are almost 40 μm, which are far larger than the grain size of the FeNiCoCrMn HEA. A lower growth rate at 800°C annealing is observed in the FeNiCoCrMn HEA and the grain size increases from 5 μm to 11 μm when increasing the annealing time from 0.5 to 24 hours. The resistance to grain growth is exceptional in the FeNiCoCrMn HEA as compared to that of FeNiCo and Ni, when annealing was performed at 800°C.

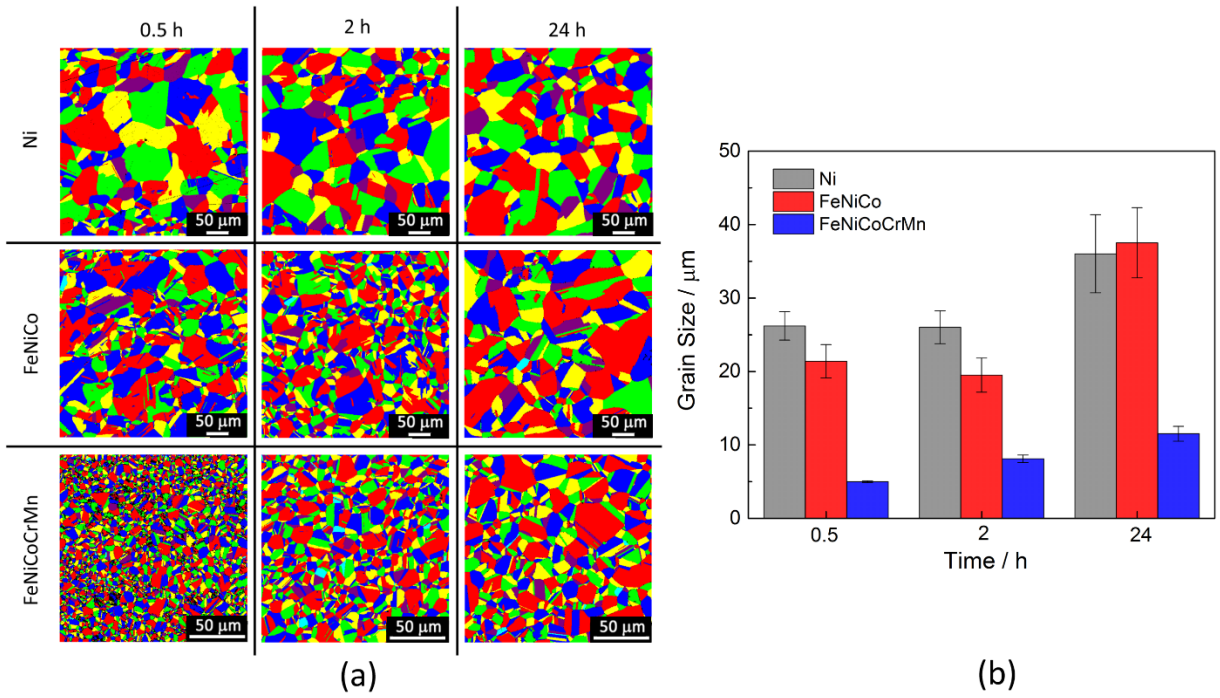

Figure 6. (a) EBSD grain orientation maps, (b) average grain sizes after annealing at 800°C for 0.5, 2 and 24 hours of the Ni, FeNiCo and FeNiCoCrMn samples.

The isothermal annealing at 800 °C after 85% reduction of cross sectional-area gives rise to the microstructural evolution, including recrystallization, grain growth, and twin formation. After the annealing at 800°C for 0.5 hours, the fully-recrystallized microstructures were observed in the Ni, FeNiCo and FeNiCoCrMn samples; however, minor fractions of substructured grains were detected by EBSD measurement. Laplanche et al. [20] and F. Otto [23] also observed that a complete recrystallization in the FeNiCoCrMn HEA was obtained at 800 °C after applying a high degree of cold working. Also, the microstructural attributes, such as grain size and twin density, are observed to be strongly dependent on the compositional composition. For instance, the smallest grain size was established in the FeNiCoCrMn HEA specimen recrystallized at 800 °C for 0.5 hours. This can be explained by a higher dislocation density (related to a greater number of nucleation sites for recrystallization) generated during the swaging process than the pure Ni and FeNiCo alloy samples. This also relates to low stacking fault energy, which is associated with the chemical composition of the FeNiCoCrMn HEA.

The longer annealing at 800 °C for up to 24 hours leads to a grain growth for all samples, but at different growth rates. Based on the grain sizes of the recrystallized samples at 800 °C for 0.5 hours, one can expect that the grain growth rate of the FeNiCoCrMn HEA specimen (~ 5 µm) would be faster than the

pure Ni (~ 26 μm) and FeNiCo alloy (~ 21 μm) samples. However, our experimental results reveal the opposite trend that grain growth rate of the FeNiCoCrMn HEA is lower than the FeNiCo alloy and pure Ni. This is because the grain growth process involves kinetic processes, such as diffusion or grain-boundary migration. In particular, the solute drag associated with a large number of the constituent elements could retard grain boundary migration during grain growth [50]. Therefore, it could be assumed that during annealing the grain boundary migration in the FeNiCoCrMn HEA is slower than those in the ternary FeNiCo and pure Ni. In addition to the solute drag effect, the SFE could play a role in controlling the kinetic processes, such as rate of recovery, recrystallization, and grain growth [47]. For instance, the low SFE is effective to reduce the rate of dislocation climb and cross-slip, which results in a decrease in the rate of grain growth for the FeNiCoCrMn HEA.

The overall observation on the microstructural evolutions during the isothermal annealing suggested that not only the number of constituent elements, but the chemical composition also had an effect. The results demonstrated that the sizes of recrystallized grains between the Ni and FeNiCo samples, which consist of different number of constituent elements, were not significantly different during the isothermal annealing. This indicated similar grain growth kinetics between the Ni and FeNiCo samples. Additionally, the ternary CoCrNi alloy has been recently reported to obtain fine grained microstructure after thermomechanical treatment and showed slow grain growth during annealing similar to the FeNiCoCrMn HEA [11, 17, 51]. It is reported that the diffusion kinetics evolved in grain growth are correlated with the lattice potential energy fluctuation which is possibly resulted by atomic size misfit and electronic disorder [51, 52]. For the electronic disorder, it was indicated from the experimental investigations [53, 54] that the FeNiCoCrMn HEA had a distortion of electronic structure, whereas the Ni sample and FeNiCo alloy presented a smaller degree of the distortion. For the aspect of atomic size misfit, the atomic size misfits of these samples are not significantly large due to similar atomic size of their constituent elements (Fe, Ni, Co, Cr and Mn). However, the atomic size misfit of the FeNiCoCrMn HEA (1.12%) is larger than the values of FeNiCo alloy (0.65%) and pure Ni (0%). The distortion of electronic structure and the larger atomic size misfit of the FeNiCoCrMn HEA are expected to lead to slower grain growth kinetic than the FeNiCo and Ni samples. It can be said that the microstructural evolution during the isothermal annealing depends on the type and the combination of constituent elements, rather than the number of constituent elements.

4. Conclusions

The microstructural responses (dislocation density, annealing twin density, recrystallization, and grain growth) of the pure Ni, ternary FeNiCo alloy, and FeNiCoCrMn HEA to the thermomechanical treatments were investigated via synchrotron X-ray diffraction, SEM, and EBSD. These materials were

subjected to cold swaging, followed by isothermal annealing at 800 °C for up to 24 hours. During the thermomechanical treatments, the pure Ni, ternary FeNiCo alloy, and FeNiCoCrMn HEA showed a FCC solid solution phase, while apparent differences in the dislocation density and behavior of recrystallization and grain growth were observed, as follows.

(1) The cold-swaging process with 85% cross-sectional area reduction introduced the higher dislocation density in the FeNiCoCrMn HEA (12.0×10^{14} m^{-2}) compared to the FeNiCo alloy (6.7×10^{14} m^{-2}) and pure Ni (2.8×10^{14} m^{-2}). The level of dislocation accumulation is related to the number of constituent elements and the intrinsic properties (i.e. stacking fault energy).

(2) After annealing at 800 °C for 0.5 hours, the large fraction of recrystallized grains and no deformed grains were observed in all samples. The as-annealed FeNiCoCrMn HEA sample possessed the smaller grain size (~ 5 μm) than that of the FeNiCo alloy (~ 21 μm) and pure Ni sample (~ 26 μm).

(3) A higher amount of twin boundaries was developed for the FeNiCoCrMn HEA than other alloys during the recrystallization process.

(4) The rate of the grain growth was observed to be lowest for the FeNiCoCrMn HEA, but the grain growth behaviors of the FeNiCo and Ni samples were similar during isothermal annealing at 800°C for up to 24 hours. It indicated that the type and combination of constituent elements have also important effects on the microstructural evolution.

Acknowledgement

Financial supports of Graduate Academy of TU Dresden and the Deutsche Forschungsgemeinschaft DFG (HA7796/1-1 and FR1714/7-1) are gratefully acknowledged. The authors thank C. Blum, D. Seifert and S. Donath for technical assistance.

Data availability

The raw/processed data required to reproduce these findings cannot be shared at this time as the data also forms part of an ongoing study.

References

[1] B. Cantor, I.T.H. Chang, P. Knight, A.J.B. Vincent, Microstructural development in equiatomic multicomponent alloys, Mater. Sci. Eng. A., 375–377 (2004) 213-218. http://dx.doi.org/10.1016/j.msea.2003.10.257

[2] M.C. Gao, J.W. Yeh, P.K. Liaw, Y. Zhang, High-entropy alloys: fundamentals and applications, Springer Nature, Switzerland, 2016.
[3] B.S. Murty, J.W. Yeh, S. Ranganathan, High-entropy alloys, Butterworth-Heinemann, Boston, 2014.
[4] E.J. Pickering, N.G. Jones, High-entropy alloys: a critical assessment of their founding principles and future prospects, Int. Mater. Rev., 61 (2016) 183-202. http://dx.doi.org/10.1080/09506608.2016.1180020
[5] D.B. Miracle, O.N. Senkov, A critical review of high entropy alloys and related concepts, Acta Mater., 122 (2017) 448-511. https://doi.org/10.1016/j.actamat.2016.08.081
[6] F. Otto, Y. Yang, H. Bei, E.P. George, Relative effects of enthalpy and entropy on the phase stability of equiatomic high-entropy alloys, Acta Mater., 61 (2013) 2628-2638. http://dx.doi.org/10.1016/j.actamat.2013.01.042
[7] A. Gali, E.P. George, Tensile properties of high- and medium-entropy alloys, INTERMETALLICS, 39 (2013) 74-78. https://doi.org/10.1016/j.intermet.2013.03.018
[8] R. Kozak, A. Sologubenko, W. Steurer, Single-phase high-entropy alloys – an overview, Z. Kristallogr. Cryst. Mater., 230 (2015) 55-68. http://dx.doi.org/10.1515/zkri-2014-1739
[9] S.J. Mary, N. Rajan, R. Epshiba, High entropy alloys properties and its applications–an overview, Eur. Chem. Bull., 4 (2015) 279-284.
[10] W.H. Liu, Y. Wu, J.Y. He, T.G. Nieh, Z.P. Lu, Grain growth and the Hall–Petch relationship in a high-entropy FeCrNiCoMn alloy, Scr. Mater., 68 (2013) 526-529. https://doi.org/10.1016/j.scriptamat.2012.12.002
[11] Z. Wu, H. Bei, F. Otto, G.M. Pharr, E.P. George, Recovery, recrystallization, grain growth and phase stability of a family of FCC-structured multi-component equiatomic solid solution alloys, INTERMETALLICS, 46 (2014) 131-140. http://dx.doi.org/10.1016/j.intermet.2013.10.024
[12] N.D. Stepanov, D.G. Shaysultanov, R.S. Chernichenko, N.Y. Yurchenko, S.V. Zherebtsov, M.A. Tikhonovsky, G.A. Salishchev, Effect of thermomechanical processing on microstructure and mechanical properties of the carbon-containing CoCrFeNiMn high entropy alloy, J. Alloys Compd., 693 (2017) 394-405. https://doi.org/10.1016/j.jallcom.2016.09.208
[13] G. Laplanche, A. Kostka, O.M. Horst, G. Eggeler, E.P. George, Microstructure evolution and critical stress for twinning in the CrMnFeCoNi high-entropy alloy, Acta Mater., 118 (2016) 152-163. https://doi.org/10.1016/j.actamat.2016.07.038
[14] Z. Wu, H. Bei, G.M. Pharr, E.P. George, Temperature dependence of the mechanical properties of equiatomic solid solution alloys with face-centered cubic crystal structures, Acta Mater., 81 (2014) 428-441. https://doi.org/10.1016/j.actamat.2014.08.026

[15] H.Y. Diao, R. Feng, K.A. Dahmen, P.K. Liaw, Fundamental deformation behavior in high-entropy alloys: An overview, Curr. Opin. Solid State Mater. Sci., 21 (2017) 252-266. https://doi.org/10.1016/j.cossms.2017.08.003

[16] J.-W. Yeh, Physical metallurgy of high-entropy alloys, JOM, 67 (2015) 2254-2261. https://doi.org/10.1007/s11837-015-1583-5

[17] G. Laplanche, A. Kostka, C. Reinhart, J. Hunfeld, G. Eggeler, E.P. George, Reasons for the superior mechanical properties of medium-entropy CrCoNi compared to high-entropy CrMnFeCoNi, Acta Mater., 128 (2017) 292-303. https://doi.org/10.1016/j.actamat.2017.02.036

[18] W. Woo, E.W. Huang, J.-W. Yeh, H. Choo, C. Lee, S.-Y. Tu, In-situ neutron diffraction studies on high-temperature deformation behavior in a CoCrFeMnNi high entropy alloy, INTERMETALLICS, 62 (2015) 1-6. http://dx.doi.org/10.1016/j.intermet.2015.02.020

[19] F. Otto, A. Dlouhý, C. Somsen, H. Bei, G. Eggeler, E.P. George, The influences of temperature and microstructure on the tensile properties of a CoCrFeMnNi high-entropy alloy, Acta Mater., 61 (2013) 5743-5755. https://doi.org/10.1016/j.actamat.2013.06.018

[20] G. Laplanche, O. Horst, F. Otto, G. Eggeler, E.P. George, Microstructural evolution of a CoCrFeMnNi high-entropy alloy after swaging and annealing, J. Alloys Compd., 647 (2015) 548-557. https://doi.org/10.1016/j.jallcom.2015.05.129

[21] P.R. Rios, F. Siciliano Jr, H.R.Z. Sandim, R.L. Plaut, A.F. Padilha, Nucleation and growth during recrystallization, Materials Research, 8 (2005) 225-238.

[22] S. Praveen, J. Basu, S. Kashyap, R.S. Kottada, Exceptional resistance to grain growth in nanocrystalline CoCrFeNi high entropy alloy at high homologous temperatures, J. Alloys Compd., 662 (2016) 361-367. https://doi.org/10.1016/j.jallcom.2015.12.020

[23] F. Otto, N.L. Hanold, E.P. George, Microstructural evolution after thermomechanical processing in an equiatomic, single-phase CoCrFeMnNi high-entropy alloy with special focus on twin boundaries, INTERMETALLICS, 54 (2014) 39-48. https://doi.org/10.1016/j.intermet.2014.05.014

[24] T. Maitland, S. Sitzman, Electron Backscatter Diffraction (EBSD) Technique and Materials Characterization Examples, in: W. Zhou, Z.L. Wang (Eds.) Scanning Microscopy for Nanotechnology: Techniques and Applications, Springer New York, 2007, pp. 41-75.

[25] X.-M. Chen, Y.C. Lin, F. Wu, EBSD study of grain growth behavior and annealing twin evolution after full recrystallization in a nickel-based superalloy, J. Alloys Compd., 724 (2017) 198-207. https://doi.org/10.1016/j.jallcom.2017.07.027

[26] H. Liu, M. Gao, D.G. Harlow, R.P. Wei, Grain boundary character, and carbide size and spatial distribution in a ternary nickel alloy, Scr. Metall. Mater., 32 (1995) 1807-1812. https://doi.org/10.1016/0956-716X(95)00015-N

[27] J. Rodríguez-Carvajal, Recent advances in magnetic structure determination by neutron powder diffraction, Physica B, 192 (1993) 55-69. https://doi.org/10.1016/0921-4526(93)90108-I

[28] H.M. Rietveld, A profile refinement method for nuclear and magnetic structures, J. Appl. Crystallogr., 2 (1969) 65-71. doi:10.1107/S0021889869006558

[29] A. Khorsand Zak, W.H. Abd. Majid, M.E. Abrishami, R. Yousefi, X-ray analysis of ZnO nanoparticles by Williamson–Hall and size–strain plot methods, Solid State Sci., 13 (2011) 251-256. https://doi.org/10.1016/j.solidstatesciences.2010.11.024

[30] G.K. Williamson, W.H. Hall, X-ray line broadening from filed aluminium and wolfram, Acta Metall., 1 (1953) 22-31. https://doi.org/10.1016/0001-6160(53)90006-6

[31] G.K. Williamson, R.E. Smallman, III. Dislocation densities in some annealed and cold-worked metals from measurements on the X-ray debye-scherrer spectrum, Phil. Mag., 1 (1956) 34-46. http://dx.doi.org/10.1080/14786435608238074

[32] W.F. Hosford, Mechanical behavior of materials, Cambridge University Press, Cambridge, 2005.

[33] R.E. Smallman, R.J. Bishop, Modern physical metallurgy and materials engineering, Butterworth-Heinemann, Oxford, 1999.

[34] C.B. Carter, S.M. Holmes, The stacking-fault energy of nickel, Phil. Mag., 35 (1977) 1161-1172. http://dx.doi.org/10.1080/14786437708232942

[35] A.J. Zaddach, C. Niu, C.C. Koch, D.L. Irving, Mechanical properties and stacking fault energies of NiFeCrCoMn high-entropy alloy, JOM, 65 (2013) 1780-1789. https://doi.org/10.1007/s11837-013-0771-4

[36] H. Oh, D. Ma, G. Leyson, B. Grabowski, E. Park, F. Körmann, D. Raabe, Lattice Distortions in the FeCoNiCrMn High Entropy Alloy Studied by Theory and Experiment, Entropy, 18 (2016) 321. https://doi:10.3390/e18090321

[37] L.R. Owen, E.J. Pickering, H.Y. Playford, H.J. Stone, M.G. Tucker, N.G. Jones, An assessment of the lattice strain in the CrMnFeCoNi high-entropy alloy, Acta Mater., 122 (2017) 11-18. http://dx.doi.org/10.1016/j.actamat.2016.09.032

[38] H. Parvin, M. Kazeminezhad, Development a dislocation density based model considering the effect of stacking fault energy: Severe plastic deformation, Comput. Mater. Sci., 95 (2014) 250-255. https://doi.org/10.1016/j.commatsci.2014.07.027

[39] L. Vitos, J.O. Nilsson, B. Johansson, Alloying effects on the stacking fault energy in austenitic stainless steels from first-principles theory, Acta Mater., 54 (2006) 3821-3826. https://doi.org/10.1016/j.actamat.2006.04.013

[40] B. Cai, S. Ren, S. Zhou, P. Li, W. Lv, J. Tao, X. Zhu, Effects of stacking fault energy on the deformation mechanisms and mechanical properties of Cu and Cu alloys processed by rolling at different temperatures, Indian J. Eng. Mater. Sci., 22 (2015) 399-406.

[41] W.G. Nöhring, W.A. Curtin, Dislocation cross-slip in fcc solid solution alloys, Acta Mater., 128 (2017) 135-148. https://doi.org/10.1016/j.actamat.2017.02.027

[42] D.M. Symons, Hydrogen embrittlement of Ni-Cr-Fe alloys, Metall. Mater. Trans. A, 28 (1997) 655-663. http://dx.doi.org/10.1007/s11661-997-0051-4

[43] D.J. Siegel, Generalized stacking fault energies, ductilities, and twinnabilities of Ni and selected Ni alloys, Appl. Phys. Lett., 87 (2005) 121901. https://doi.org/10.1063/1.2051793

[44] N.D. Stepanov, D.G. Shaysultanov, M.S. Ozerov, S.V. Zherebtsov, G.A. Salishchev, Second phase formation in the CoCrFeNiMn high entropy alloy after recrystallization annealing, Mater. Lett., 185 (2016) 1-4. http://dx.doi.org/10.1016/j.matlet.2016.08.088

[45] F.J. Humphreys, J.W. Martin, The effect of dispersed phases upon dislocation distributions in plastically deformed copper crystals, The Philosophical Magazine: A Journal of Theoretical Experimental and Applied Physics, 16 (1967) 927-957. 10.1080/14786436708229685

[46] V. Randle, D. Horton, Grain growth phenomena in nickel, Scr. Metall. Mater., 31 (1994) 891-895. https://doi.org/10.1016/0956-716X(94)90498-7

[47] A. Rollett, F.J. Humphreys, G.S. Rohrer, M. Hatherly, Recrystallization and related annealing phenomena, Elsevier, Netherlands, 2004.

[48] B.-R. Chen, A.-C. Yeh, J.-W. Yeh, Effect of one-step recrystallization on the grain boundary evolution of CoCrFeMnNi high entropy alloy and its subsystems, Sci. Rep., 6 (2016) 1-9. http://dx.doi.org/10.1038/srep22306

[49] C.S. Pande, M.A. Imam, B.B. Rath, Study of annealing twins in fcc metals and alloys, Metall. Trans. A, 21 (1990) 2891-2896. http://dx.doi.org/10.1007/bf02647209

[50] E. Hersent, K. Marthinsen, E. Nes, A solute pinning approach to solute drag in multi-component solid solution alloys, MNSMS, 4 (2014) 8-13. http://dx.doi.org/10.4236/mnsms.2014.41002

[51] G. Dan Sathiaraj, W. Skrotzki, A. Pukenas, R. Schaarschuch, R. Jose Immanuel, S.K. Panigrahi, J. Arout Chelvane, S.S. Satheesh Kumar, Effect of annealing on the microstructure and texture of cold rolled CrCoNi medium-entropy alloy, INTERMETALLICS, 101 (2018) 87-98. https://doi.org/10.1016/j.intermet.2018.07.014

[52] K.Y. Tsai, M.H. Tsai, J.W. Yeh, Sluggish diffusion in Co–Cr–Fe–Mn–Ni high-entropy alloys, Acta Mater., 61 (2013) 4887–4897. http://dx.doi.org/10.1016/j.actamat.2013.04.058

[53] Y. Zhang, K. Jin, H. Xue, C. Lu, R.J. Olsen, L.K. Beland, M.W. Ullah, S. Zhao, H. Bei, D.S. Aidhy, G.D. Samolyuk, L. Wang, M. Caro, A. Caro, G.M. Stocks, B.C. Larson, I.M. Robertson, A.A. Correa, W.J. Weber, Influence of chemical disorder on energy dissipation and defect evolution in advanced alloys, J. Mater. Res., 31 (2016) 2363-2375. 10.1557/jmr.2016.269

[54] K. Jin, B.C. Sales, G.M. Stocks, G.D. Samolyuk, M. Daene, W.J. Weber, Y. Zhang, H. Bei, Tailoring the physical properties of Ni-based single-phase equiatomic alloys by modifying the chemical complexity, Sci. Rep., 6 (2016) 20159. 10.1038/srep20159

Figure captions

Figure 1. Synchrotron X-ray diffraction patterns of the as-swaged FeNiCoCrMn, FeNiCo and pure Ni samples.

Figure 2. (a) Williamson-Hall analysis and (b) dislocation density of the as-swaged FeNiCoCrMn HEA, FeCoNi and pure Ni samples.

Figure 3. SE-SEM micrographs of (a) Ni, (b) FeNiCo and (c) FeNiCoCrMn alloys, annealed at 800°C for 0.5 hours. The yellow circles indicate the smaller grains surrounded by larger grains and the white arrows point Cr-rich particles.

Figure 4. Grain size distribution of Ni, FeNiCo and FeNiCoCrMn samples after the annealing at 800°C for 0.5 hours.

Figure 5. EBSD grain boundary maps of (a) Ni, (b) FeNiCo and (c) FeNiCoCrMn alloys, annealed at 800°C for 0.5 hours.

Figure 6. (a) EBSD grain orientation maps, (b) average grain sizes after annealing at 800°C for 0.5, 2 and 24 hours of the Ni, FeNiCo and FeNiCoCrMn samples.

Table

Table 1 lattice parameters (a), Burgers vector (b), grain (crystallite) size (D_v), lattice strain (ε), dislocation density (ρ) and stacking fault energy (γ) of as-swaged samples and homologous temperature for annealing at 800°C (1073K)

Alloys	a (Å)	b (Å)	D_v (nm)	ε (%)	ρ (x 10^{14} m^{-2})	γ (mJ/m^2)	T/T_m (T =1073K)
Ni	3.521	2.490	98	0.104	2.831	120 - 130 [34]	0.62
FeNiCo	3.569	2.524	125	0.163	6.719	31 [2]	0.63
FeNiCoCrMn	3.594	2.541	156	0.220	12.018	18 - 27 [35]	0.69

Table 2 Microstructural analysis of the studied samples after the annealing at 800°C for 0.5 hours, evaluated on EBSD maps.

Alloys	Grain Size (μm)	Residual strain analysis			Twin Σ3 (%)
		Undeformed (%)	Substructured (%)	Deformed (%)	
Ni	26 ± 2	92	8	0	6
FeNiCo	21 ± 2	91	9	0	16
FeNiCoCrMn	5 ± 0	80	20	0	21